NREL
NATIONAL RENEWABLE ENERGY LABORATORY

Turbine Inflow Characterization at the National Wind Technology Center

Preprint

A. Clifton, S. Schreck, G. Scott, and N. Kelley
National Renewable Energy Laboratory

J. Lundquist
National Renewable Energy Laboratory and
University of Colorado at Boulder

To be presented at the 50th AIAA Aerospace Sciences Meeting
Nashville, Tennessee
January 9-12, 2012

NREL is a national laboratory of the U.S. Department of Energy, Office of Energy Efficiency & Renewable Energy, operated by the Alliance for Sustainable Energy, LLC.

Conference Paper
NREL/CP-5000-53525
January 2012

Contract No. DE-AC36-08GO28308

NOTICE

The submitted manuscript has been offered by an employee of the Alliance for Sustainable Energy, LLC (Alliance), a contractor of the US Government under Contract No. DE-AC36-08GO28308. Accordingly, the US Government and Alliance retain a nonexclusive royalty-free license to publish or reproduce the published form of this contribution, or allow others to do so, for US Government purposes.

This report was prepared as an account of work sponsored by an agency of the United States government. Neither the United States government nor any agency thereof, nor any of their employees, makes any warranty, express or implied, or assumes any legal liability or responsibility for the accuracy, completeness, or usefulness of any information, apparatus, product, or process disclosed, or represents that its use would not infringe privately owned rights. Reference herein to any specific commercial product, process, or service by trade name, trademark, manufacturer, or otherwise does not necessarily constitute or imply its endorsement, recommendation, or favoring by the United States government or any agency thereof. The views and opinions of authors expressed herein do not necessarily state or reflect those of the United States government or any agency thereof.

Available electronically at http://www.osti.gov/bridge

Available for a processing fee to U.S. Department of Energy
and its contractors, in paper, from:

U.S. Department of Energy
Office of Scientific and Technical Information

P.O. Box 62
Oak Ridge, TN 37831-0062
phone: 865.576.8401
fax: 865.576.5728
email: mailto:reports@adonis.osti.gov

Available for sale to the public, in paper, from:

U.S. Department of Commerce
National Technical Information Service
5285 Port Royal Road
Springfield, VA 22161
phone: 800.553.6847
fax: 703.605.6900
email: orders@ntis.fedworld.gov
online ordering: http://www.ntis.gov/help/ordermethods.aspx

Cover Photos: (left to right) PIX 16416, PIX 17423, PIX 16560, PIX 17613, PIX 17436, PIX 17721

Printed on paper containing at least 50% wastepaper, including 10% post consumer waste.

Turbine Inflow Characterization at the National Wind Technology Center

Andrew Clifton* Scott Schreck † George Scott ‡

Neil Kelley §

National Renewable Energy Laboratory, Golden, CO 80401 U.S.A.

Julie K. Lundquist ¶

National Renewable Energy Laboratory, Golden, CO 80401 U.S.A.

University of Colorado at Boulder, Boulder, CO, 80309 U.S.A.

Utility-scale wind turbines operate in dynamic flows that can vary significantly over timescales from less than a second to several years. To better understand the inflow to utility-scale turbines, two inflow towers were installed and commissioned at the National Renewable Energy Laboratory's (NREL) National Wind Technology Center near Boulder, Colorado, in 2011. These towers are 135 m tall and instrumented with a combination of sonic anemometers, cup anemometers, wind vanes, and temperature measurements to characterize the inflow wind speed and direction, turbulence, stability and thermal stratification to two utility-scale turbines. Herein, we present variations in mean and turbulent wind parameters with height, atmospheric stability, and as a function of wind direction that could be important for turbine operation as well as persistence of turbine wakes. Wind speed, turbulence intensity, and dissipation are all factors that affect turbine performance. Our results show that these all vary with height across the rotor disk, demonstrating the importance of measuring atmospheric conditions that influence wind turbine performance at multiple heights in the rotor disk, rather than relying on extrapolation from lower levels.

Nomenclature

C_p = specific heat capacity at constant pressure, 1005 J Kg^{-1} K^{-1}
e = vapor pressure
f = cyclical frequency
g = acceleration due to gravity, 9.81 m/s^2
I = turbulence intensity
L = Monin-Obukhov length
P = barometric pressure
q = specific humidity
Q_0 = surface heat flux
R = gas constant of dry air, 287 J Kg^{-1} K^{-1}
Ri = gradient Richardson number
Ri_S = speed Richardson number
T = absolute temperature
T_d = dew point temperature

*Senior Engineer, National Wind Technology Center, Golden, CO.
†Principal Engineer, National Wind Technology Center, Golden, CO.
‡Scientist, National Wind Technology Center, Golden, CO.
§Principal Scientist, National Wind Technology Center, Golden, CO.
¶Assistant Professor, Department of Atmospheric and Oceanic Sciences, University of Colorado at Boulder, Boulder, CO, 80309 U.S.A.

T_v = virtual temperature
U = stream-wise velocity
u_* = friction velocity
u_m = zonal (west-east) wind component
v_m = meridional (south-north) wind component
w = vertical wind component
z = height above ground

Symbols
ϵ = dissipation rate
κ = Von Kármán constant, 0.41
θ = potential temperature
θ_v = virtual potential temperature
ζ = ratio z/L

I. Introduction

Modern utility-scale wind turbines have hub heights of 80 m or more, and rotor diameters upwards of 100 m. Since the 1980s there has been a trend of continuous growth in turbine size and power rating.[1] In 2011, several manufacturers announced turbines with hubs at more than 100 m above ground and rotor diameters of more than 120 m. Wind turbines operate in an atmospheric boundary layer characterized by turbulence. This layer experiences significant changes in heat fluxes at the lower boundary, switching from convective conditions during the day to stable conditions overnight. The change in stability is known to alter turbulence (which varies by site as well[2]), impact turbine performance[3] and also affects turbine loads.[4] The rotation of the earth, manifested in the Coriolis effect, also influences winds, leading to a change in wind direction with height that can be further complicated by synoptic forcing. Stability, wind direction veer, and jets all represent a departure from the predictable flow suggested by canonical power or logarithmic law flows.[5] This combination of continued growth in turbine size and dynamic boundary layer conditions requires careful, *coupled* monitoring of turbine behavior and wind inflow conditions to understand and improve performance and reliability.[6]

The importance of atmospheric stability and coherent turbulent structures in wind for turbine behavior was shown by a series of measurements in a large, 41-row wind farm in the San Gorgonio Pass, California. Observations there showed that upwind turbines, particularly under stable night-time conditions, enhanced turbulence within the turbine array.[7] Wavelet analysis methods revealed that organized or coherent turbulence was responsible for an increase in damage-equivalent loading. This effect is expected to increase for large arrays of turbines.[7]

A later series of experiments at the National Wind Technology Center (NWTC) used an array of sonic anemometers to measure inflow to the 42-m-diameter, 600-kW Advanced Research Turbine (ART). These experiments were part of the Long-Term Inflow and Structural Testing (LIST) program to establish the sensitivity of wind turbines to inflow conditions, quantify the impact of boundary layer stability, and develop a boundary layer simulation tool. Results from those tests suggested that turbine loads were sensitive to coherent structures found in stable nocturnal boundary layers.[4,8] The authors suggested that this would become ever more important as turbines increased in size and were more heavily impacted by these flow phenomena, particularly below low-level jets.

The Lamar Low-Level Jet Program (LLLJP) measurement campaign quantified the frequency and magnitude of the low-level jet near Lamar in southeast Colorado in 2003 using a combination of an instrumented tower, SODAR, and NOAA's three-dimensional scanning wind LIDAR, the High Resolution Doppler LIDAR (HRDL). Results showed that the jet was responsible for the formation of Kelvin-Helmholtz instabilities (KHI) at elevations typical of modern turbine rotor disks.[9,10] The Kelvin-Helmholtz instabilities ultimately collapse to create coherent turbulent structures that then contribute to significantly enhanced turbine loads. These flow phenomena occur throughout the U.S. Midwest in states that represent a significant proportion of the installed and future potential wind energy capacity in the United States.

A comparison of atmospheric data from the San Gorgonio and LIST measurement campaigns showed that loads peaked when the local turbine-layer Richardson number was in the range $0.01 > Ri_{TL} > 0.05$.[10] This range corresponds with the formation of Kelvin-Helmholtz Instabilities and peak values of the coherent

turbulent kinetic energy.

The stochastic wind field simulator TurbSim was created using lessons learned from San Gorgonio, LIST, and LLLJP to produce a desktop simulation of a realistic atmospheric boundary layer.[11] This tool generates a wind field with similar statistical properties to those seen during these studies and is designed to be interfaced to turbine aerostructural models to estimate structural loading. TurbSim can also be used to generate boundary conditions for computational fluid dynamics calculations.[12]

The National Wind Technology Center is situated about 20 miles to the northwest of Denver, Colorado, at the foot of the Front Range at an elevation of around 1850 m above sea level. Winds on site are dominated by strong westerly winds, typically resulting from a drainage flow out of the nearby Eldorado Canyon,[13] visible in the upper right quadrant of Figure 1. The NWTC is flat and undeveloped, and forms a "wind reservation" with very uniform surface cover to help reduce the variation seen in the wind profiles at the east end of the site by the time they reach the turbine test stands at the west end of the site. Although the mean wind speed on site is low, winds can be extremely gusty and turbulent. For this reason, and because of the NWTC's accreditation as a turbine test location with the American Association for Laboratory Accreditation (A2LA), the site is a preferred location for many manufacturers to test turbines and establish performance, reliability, and survivability. The U.S. Department of Energy (DOE) installed the DOE/GE 1.5-MW turbine with 80-m hub height and 78-m rotor diameter at the NWTC in 2009. Three other utility-scale turbines have been installed on site since then, including a Siemens 2.3-MW turbine in 2009, and an Alstom 3-MW Eco100 and Gamesa 2-MW G97 turbine in 2011.

Figure 1. The view to the northwest across the NWTC in May 2011. Three utility-scale turbines are in the foreground of the picture to the left and right. The 38-m hub height Advanced Research Turbines are slightly set back. Photo by Dennis Schroeder, NREL/PIX 19018.

A range of inflow data has been collected at the NWTC. An 80-m tower at the west end of the site monitors inflow from the mountains, from where the strongest winds typically come. This tower, designated 'M2', has been in operation since 1996, and data are publicly available online. Inflow into the two- and three-bladed Advanced Research Turbines (ART) is monitored at several heights by cup anemometers and vanes, and turbulence is measured using a sonic anemometer at the hub height. When turbines are undergoing performance testing, masts are installed upstream and instrumented with hub-height cup anemometers. These cups are mounted on long booms and calibrated to relevant standards. Other towers are instrumented specifically for cooperative research projects or for certain tasks, such as in the LIST experiments. Several remote sensing devices have been used on site over the last 20 years, including commercial and research LIDAR and SODAR systems.[13–16] Drawing on the lessons learned from the San Gorgonio, LIST, and LLLJP studies, 135-m inflow monitoring towers were installed upwind of two of the NWTC test turbines in late 2010. A key goal of the tower measurements is to quantify turbulence and thermal stratification for the

validation of the TurbSim model. Coupled measurements of inflow and turbine conditions will be analyzed in detail when high-load events occur.

A summary of inflow monitoring systems that operated during 2011, and the meteorological variable they measured, is given in Table 1. Systems that operated temporarily as part of measurement campaigns are indicated. Other meteorological observation systems operate at the NWTC, including precipitation measurements, barometric pressure, atmospheric electric field strength, relative humidity and incoming solar radiation.

Site	Purpose	Device	Variables	N	Heights (m)	Operates
M2	Tower	Cup anemometer, wind vane, thermistors.	U, T, WD	6	2-80	All year
ART	Inflow Tower	Cup anemometer, wind vane	U, T, WD	3	18 - 58	Campaigns
		Sonic anemometer	u, v, w, T	1	38	Campaigns
M4	Inflow Tower	Cup anemometer	U	1	80	
		Cup anemometer, wind vane	U, T, WD	5	3-134	All year
		Sonic anemometer	u, v, w, T	6	15-131	All year
M5	Inflow Tower	Cup anemometer	U	6	30-130	
		Cup anemometer, wind vanes	U, T, WD	5	3-122	All year
		Sonic anemometer	u, v, w, T	6	15-119	All year
Various	Turbine testing	Cup anemometer, wind vane	U, WD	-	hub	Campaigns
	Research	Scanning LIDAR	u, v, w	-	to 1,000 m	Campaigns
	Research	Profiling LIDAR	U, WD, w	-	to 200 m	Campaigns[16]
	Research	Profiling SODAR	U, WD, w	-	to 200 m	Campaigns
	Research	Radiometer	T	-	to 2,000 m	Campaigns[16]

Table 1. Sources of inflow data at the NWTC in 2011. Measurement heights are nominal values. Measured parameters include the stream-wise velocity U; temperature T; wind direction WD and orthogonal wind vectors u, v, and w at N heights. Research LIDAR and SODAR have adjustable measurement heights to the maximum range given in the table.

In this paper we show how the 135-m meteorological towers and measurement systems have been specially designed to capture relevant flow parameters. Focusing on a month of data obtained in October and November 2011, we introduce some of the characteristics of the winds locally and discuss the implications of our measurements for turbine performance.

II. Methods

Two new 135 m meteorological towers have been installed towards the eastern side of the NWTC site. The towers are approximately 2 rotor diameters upwind of two, utility-scale wind turbines and are designed to quantify the inflow into the turbines. The towers are designated 'M4', upwind of the Siemens 2.3-MW turbine and 'M5', upwind of the DOE/GE 1.5-MW turbine.

Turbine inflow is quantified in terms of wind speed, wind direction, three-dimensional turbulence, and temperature at several heights across the turbine rotor. A full schematic of the instrumentation installed on each of the towers is shown in Figure 2. The tower instrumentation includes six three-dimensional sonic anemometers on each tower; at least 5 paired cup anemometers; vanes logarithmically distributed over the tower; and absolute, differential, and dew point temperature measurements. No humidity measurements are collected, but relative humidity is calculated from absolute and dew point temperatures (see section II.D). Instrumentation are at slightly different heights on the M4 and M5 towers to align precisely with the turbine hubs, blade tips and blade mid-span. The wind measurement devices are mounted on booms that extend horizontally from the tower structure into the prevailing winds at an angle of 285° (compare to Fig. 6). The length of the booms for the sonic anemometers are 5.8 times the width of the tower face, while cup

anemometers and sonics are on booms that are 3.5 times as long as the tower face width. We also measure barometric pressure and precipitation intensity at the ground.

The towers are stabilized by guy lines connected to anchors spaced at 120° intervals around the tower and connected to the tower structure at 6 heights (Fig. 2). The effect of these anchors is to increase the tower stiffness, reduce tower torsion, and raise the resonant frequency of the tower above the measurement frequency.

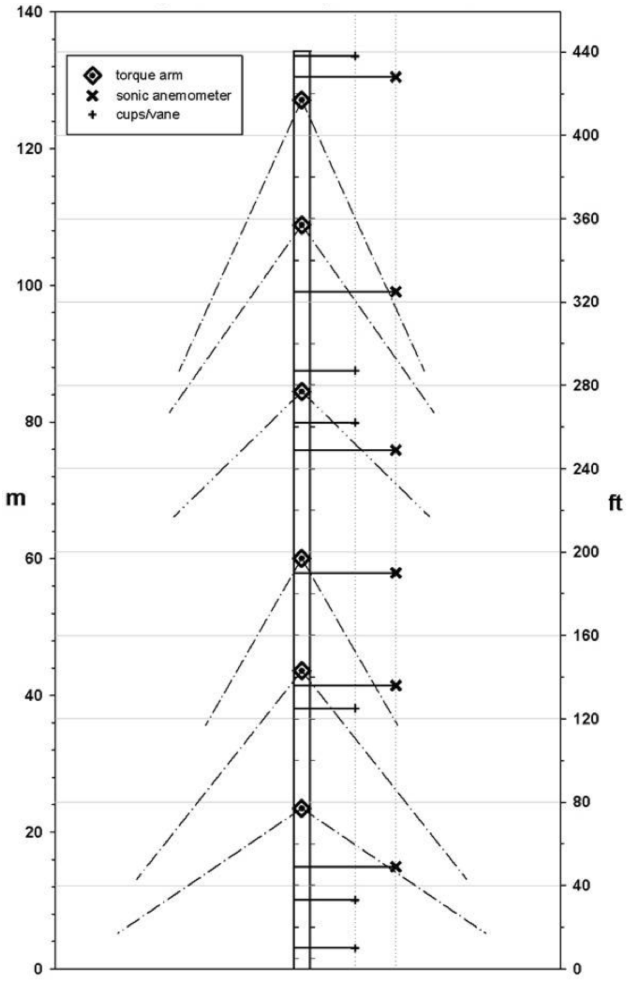

Figure 2. Schematic view of the NWTC 135-m M4 inflow monitoring tower. Boom heights are approximate. All booms face 285°.

II.A. Data acquisition and processing

Data from each tower are obtained at 20 Hz by a data acquisition system built around National Instruments LabVIEW software and National Instruments PCI boards. Separate, identical systems are used at each tower. Using duplicate systems based on standard commercially available architecture for both projects helps in commissioning and gives flexibility in adding extra instrumentation at a later date.

Our commissioning process followed several steps after the instruments were installed on the tower. First, an end-to-end signal check showed that the correct device was associated with each measurement. Other measurements established the noise floor of the system, which influences the accuracy of our measurements. Tests then confirmed the ability of the system to maintain a true 20-Hz data acquisition frequency. We also investigated the response of the system to the (simulated) failure of an instrument to ensure that failure of one device would not jeopardize data from the other instruments.

The variables listed in Table 1 are measured at 20 Hz on both of the 135-m towers, and then stored in data files of 10 minute duration. Tower data are synchronized with turbine measurements using Global

Positioning System (GPS) time signals, which allow us to link inflow winds to turbine response.

II.B. Quantifying the mean flow

The characteristics of the mean flow are calculated for each of the 10-minute data files written by the data acquisition system. A 10-minute averaging period was chosen per IEC standard 61400 for wind turbines.

We calculate the mean wind speed and direction at each height by first converting the 20-Hz wind speed U measured by the cup anemometers and direction WD measured by the vanes into 20-Hz orthogonal wind components in the meteorological zonal (west-east, u_m) and meteorological meridional (south-north, v_m) directions:

$$u_m = -U \cdot \sin\left(\frac{\pi \cdot WD}{180}\right) \tag{1}$$

$$v_m = -U \cdot \cos\left(\frac{\pi \cdot WD}{180}\right) \tag{2}$$

where positive u_m indicates a wind blowing to the east, and positive v_m is a wind blowing to the north. The mean wind speed is then calculated for each 10-minute interval as the vector mean of the orthogonal wind components:

$$\overline{U} = \left[\overline{u_m}^2 + \overline{v_m}^2\right]^{(1/2)} \tag{3}$$

The mean wind direction is the direction that the wind *comes from*, in degrees:

$$\overline{WD} = atan2(\overline{-u_m}/\overline{-v_m}) \times \frac{180}{\pi} \tag{4}$$

where the function $atan2\,(x)$ is the arc tangent of x in the range $\pm\pi$ radians.

II.C. Quantifying turbulence

Because the spectrum of turbulent fluctuations includes both large and small scales, measurement devices must be capable of resolving a wide range of wind speeds, and capturing rapid changes. We use sonic anemometers to make wind turbulence measurements as they have no inertia, a small measurement volume and can make high-frequency measurements. In comparison, the inertia of cup anemometers makes them unreliable for high-frequency turbulence measurements. Sonic anemometers measure winds in 3 orthogonal components, rather than a wind speed and direction as with cups and vanes. To calculate the mean wind vector, 10-minute blocks of measurements are rotated into the prevailing wind direction during post processing.[17] The rotation fits the measured data to find a 3-dimensional wind vector with a stream-wise component u, transverse component v and vertical component w for the 10-minute interval. The mean stream-wise velocity is maximized, while the mean transverse and vertical components are vertical over the interval.

The turbulent velocity components u', v' and w' are defined as the difference from the mean velocity component, so that $u' = u(t) - \overline{(u)}$, $v' = v(t) - \overline{(v)}$ and $w' = w(t) - \overline{(w)}$, where $\overline{(v)} = \overline{(w)} = 0$. Turbulence intensity, I, is the ratio of the standard deviation of the turbulent components to the stream-wise mean speed, expressed as a percentage.[18] For flow in the stream-wise direction (u), this percentage is

$$I(u) = \frac{\sigma\,(u')}{\overline{U}} \times 100. \tag{5}$$

Turbulence intensity is calculated only for the horizontal velocity measured by the cups, as seen in Figures 7(b) and 9(b).

The local friction velocity u_* is calculated from the turbulent velocity fluctuations measured by the sonic anemometers[18] at each height as

$$u_* = \left|\overline{u'w'}\right|^{1/2}, \tag{6}$$

where the overbar indicates the average for a ten minute interval.

Turbulence kinetic energy (TKE) is a measure of the energy in the turbulent velocity fluctuations that includes all three velocity components, rather than the turbulence intensity which only includes the streamwise component.[19] The mean TKE over a 10 minute interval is defined as

$$\mathrm{TKE} = \frac{1}{2}\overline{[u'^2 + v'^2 + w'^2]} \tag{7}$$

As was noted in the introduction, coherent turbulent kinetic energy (CTKE) is a significant contributor to turbine loads. CTKE is defined as

$$\mathrm{CTKE} = \frac{1}{2}\left([u'w']^2 + [u'v']^2 + [v'w']^2\right)^{(1/2)}. \tag{8}$$

Turbulence is generated at low frequencies by flow interacting with terrain (mechanical production), through buoyancy, and by the motion of the atmosphere. TKE is dissipated at high frequencies into heat through viscous dissipation. Understanding the power spectra of turbulence is important for turbine design, as this influences the energy that is transferred into the turbine structure. One useful measure of turbulence is the integral length scale, which describes the mean length scale of turbulent eddies in the flow. The turbulence integral length scale (Λ) for a velocity component (u', v' or w') is calculated from the time series of the turbulent velocity component. First, the characteristic time (τ_e) for the autocorrelation of the turbulent component to drop to $1/e$ is calculated. τ_e is multiplied by the mean wind speed to give the turbulence integral length scale, $\Lambda(u) = \overline{U} \times \tau_e(u)$. Because the integral length scale is of the order of the measurement height,[19] the characteristic time of flows at a turbine hub (around 80 m) at rated speed (10 to 12 m s^{-1}) is approximately 10 seconds, which can be resolved by our 20-Hz data acquisition system.

The dissipation rate ϵ is the rate at which turbulent kinetic energy is dissipated into heat at the smallest eddy scale in turbulent flow. Because this occurs at higher frequencies than can be resolved directly by the sonic anemometers, it has to be inferred from the turbulent power spectra. Here we calculate ϵ using the structure function method.[18] The structure function for a time δt is the mean squared difference between u' at times t and δt:

$$D_{AA}(\delta t) = \overline{[u'(t+\delta t) - u'(t)]^2} \tag{9}$$

Next, we calculate the ratio of the structure function to the cube root of the lag:

$$C_{v2}(\delta t) = \left[\frac{D_{AA}(\delta t)}{\left(\overline{U}\delta t\right)^{\frac{2}{3}}}\right]. \tag{10}$$

The dissipation rate is then given by:

$$\epsilon = \left[\frac{\widetilde{C_{v2}}}{2}\right]^{\frac{3}{2}} \tag{11}$$

The dissipation rate is limited to the inertial subrange by using $0.05 \leq \delta t \leq 2$, which corresponds to frequencies between 0.5 and 20 Hz. From power spectra of the turbulent velocity components (e.g. Fig. 5), this is within the inertial subrange where energy cascades from the larger scales to smaller scales at a constant rate. We will investigate other methods to quantify the dissipation rate of turbulent kinetic energy from the tower data in the future.[20]

II.D. Quantifying thermodynamic properties

To calculate the stability profile in the boundary layer, we need to quantify the air temperature and humidity profile. This requires a series of calculations, set out below. Absolute and dew point temperature and barometric pressure are measured at 3 m above ground. These values are denoted T_0, T_{d0} and P_0, respectively.

The absolute temperature profile $T(z)$ on the M4 tower is measured as the sum of T_0 and temperature differences between 3 and 26 m, 26 and 88 m, and 88 and 134 m above ground. Using differential temperature measurements with an accuracy of 0.1° gives improved accuracy compared to using two local absolute temperature measurement with a typical accuracy of 0.5°.

The local saturation vapor pressure e_s is calculated at each height from the air temperature $T(z)$ *in degrees Celsius*:

$$e_s(z) = 6.11 \times 10^{[(T(z)\cdot A)/(T(z)+B))} \tag{12}$$

where A =7.5 and B = 237.3 if $T(z) \geq 0°C$. Otherwise, A = 9.5 and B = 265.5. The actual local vapor pressure $e(z)$ is calculated from Eq. (12) using the dew point temperature T_d measured at the different heights on the tower, also in degrees celsius, instead of the absolute temperature.

The specific humidity q is the ratio of mass of water vapor to the total mass of the air.[19] It is calculated from the saturation and local vapor pressures:

$$q = 0.622\frac{e}{P} \tag{13}$$

where 0.622 is the ratio of the gas constant for dry air (287 J Kg^{-1} K^{-1}) to the gas constant for water vapor (461.5 J Kg^{-1} K^{-1}).

The virtual temperature T_v at the lowest level on the tower is given by:[19]

$$T_v = T\left(1 + 0.61q\right). \tag{14}$$

The virtual temperature and pressure at the lowest measurement height are used to calculate the pressure gradient, dP/dz from the equation of state:[19]

$$\frac{dP}{dz} = -\frac{gP_0}{RT_v} \tag{15}$$

where g is the acceleration due to gravity (9.81 m s^{-2}) and R is the gas constant of dry air.

The pressure at other observation heights (Δz above the ground) is then calculated from the measured ground pressure and the pressure gradient as $P(z) = P_0 + \Delta z \cdot dP/dz$. Once the pressure profile has been estimated, the potential temperature profile is calculated. The potential temperature Θ is the temperature that air at the ground would have if moved to a reference pressure level, P_{ref}, in this case 1000 hPa.[19] The potential temperature is:

$$\Theta\left(z\right) = T\left(z\right)\quad\frac{P_{ref}}{P\left(z\right)}\quad^{R/C_p} \tag{16}$$

where C_p is the specific heat capacity at constant pressure (1005 J Kg^{-1} K^{-1}). The ratio $R/C_p = 0.286$.

The virtual potential temperature Θ_v is the potential temperature that dry air air would require to have the same density as moist air.[19] The virtual potential temperature is:

$$\Theta_v\left(z\right) = \Theta\left(z\right)\left(1 + 0.61q\left(z\right)\right) \tag{17}$$

where q is the specific humidity at each height (Eq. 13). Profiles of T, Θ and Θ_v can then be used to visualize and quantify stability using a variety of metrics, described in II.E.

II.E. Quantifying stability

Several methods exist to quantify stratification. One method is to use the ratio of shear-driven turbulence to buoyancy-generated turbulence using the Monin-Obukhov length, L:

$$L = -\frac{u_*^3\overline{\Theta_v}}{\kappa g\overline{w'\Theta_v'}}. \tag{18}$$

The buoyancy term $\overline{w'\Theta_v'}$ in Eq. (18) is calculated from turbulent components of vertical velocity and temperature measured by the sonic anemometer, as the turbulent fluctuations of temperature measured by a sonic anemometer approximate the turbulent component of the virtual potential temperature, Θ_v'. The mean value of virtual potential temperature in Eq. (18), $\overline{\Theta_v}$, is calculated from the tower temperature and dew-point temperature profiles. The Monin-Obukhov length is usually normalized by the measurement height z (in this case the sonic anemometer height) to give the ratio $\zeta = z/L$. Locally convective conditions give $z/L < 0$, and stable conditions give $z/L > 0$, while in neutral conditions, $L \to \infty$ (Table 2).

We also quantify stability with the gradient Richardson number, which is calculated from 10-minute average temperatures and gradients of wind components and virtual potential temperature from one height

(z_1) to another (z_2).[19] In this respect, the Richardson number can be considered representative of the entire layer between z_1 and z_2. The gradient Richardson number is:

$$Ri = \frac{g}{\overline{\Theta_v}} \frac{d\overline{\Theta_v}/dz}{\left(d\overline{u_m}/dz\right)^2 + \left(d\overline{v_m}/dz\right)^2}, \tag{19}$$

where the mean virtual potential temperature between z_1 and z_2 is $<\overline{\Theta_v}>=\frac{1}{2}\left[\Theta_V\left(z_1\right)+\Theta_v\left(z_2\right)\right]$.

A simplified Richardson number has also been used in some applications.[21–23] This considers just the gradient of the mean wind speed $\overline{U}$, rather than including directional shear as in Eq. (19). To distinguish this from the gradient Richardson number, this is described in this context as the 'Speed Richardson Number', Ri_S:

$$Ri_S = \frac{g}{\overline{\Theta_v}} \frac{d\overline{\Theta_v}/dz}{d\overline{U}/dz\ ^2}. \tag{20}$$

Calculations of Ri and Ri_S from the ground to the turbine hub or tip use the mean of all of the temperature, wind speed and wind component gradients.[4]

Businger[21] found that for unstable conditions, $z/L \approx Ri_S$, while Ri_S tends towards a constant value as $z/L \to \infty$. If $\zeta = z/L$ then:

$$Ri_S = \begin{cases} 0.74\zeta \frac{(1+15\zeta)^{1/2}}{(1-9\zeta)^{1/2}} & \text{if } Ri_S < 0; \\ \frac{\zeta(0.74+4.7\zeta)}{(1+4.7\zeta)^2} & \text{if } Ri_S > 0. \end{cases} \tag{21}$$

We define several stratification classes from the Richardson number and normalized Monin-Obukhov length. These are listed in Table 2. The Richardson number bands are based on previous work on the interaction of turbines and stability,[4] and explicitly identify the slightly stable region that was found to be linked to production of CTKE. We also identify the strongly stable regime of $Ri > 0.25$ where turbulence is rapidly damped by stability.[19] A range of L has been used by different authors to define neutral conditions. When referenced back to the hub height, z_{hub}, these correspond to $|z_{hub}/L| \lesssim 0.1$.[3,24] From Eq. (21) it can be seen that for near-neutral conditions, $Ri \approx z/L$, but as stability increases, $z/L \to \infty$. Because a definition of neutral conditions as $|z/L| < 0.1$ potentially includes the slightly stable regime, we use the narrower range of $|z/L| < 0.01$ that allows us to better distinguish changes in the atmosphere in this region.

Stratification	Label	Criteria	
		Ri	z/L
Unstable	U	<-0.01	<-0.01
Neutral	N	$\lvert Ri\rvert \leq 0.01$	$\lvert z/L\rvert \leq 0.01$
Slightly stable	S1	$0.01 < \mathrm{Ri} \leq 0.05$	S: >0.01
Stable	S2	$0.05 < \mathrm{Ri} \leq 0.25$	
Strongly stable	S3	>0.25	

Table 2. Stratification classes using Ri or z/L.

II.F. Quality control

Calculating the Richardson number, Monin-Obukhov length and turbulence requires low instrument noise, regular sampling intervals and continuous sampling over long periods of time. We use high-quality, calibrated instruments and check the frequency of the data acquisition system as part of our post processing routines. Data from each instrument are checked against simple quality control measures. These quality control measures include testing for data acquisition rates of 20 Hz, and detecting flat-line data (which indicates a malfunctioning device) by checking for standard deviations that are less than 0.01 per cent. A check is also made on the number of valid data points per 10-minute interval, per channel. We chose to flag data if the number is less than 95% of the 12,000 data points that could be collected during a 10-minute interval. Flags propagate through calculations, so that if data from two channels a and b are used to calculate another value $y = f(a, b)$, output y will inherit the flags of variables a and b.

II.G. Uncertainty Estimates

An important part of any measurement is to understand the behavior of the instrumentation system and how it interacts with the property being measured. The result of this is an uncertainty estimate, which includes the uncertainty of the data acquisition process, the impact of the tower on the free stream and the inherent uncertainty of the measurement devices. The commissioning steps described in II.A allow us to quantify the uncertainty of our recorded data. We also plan to carry out studies of the extent of the distortion introduced by the tower structure into the free stream, which will allow us to quantify another part of the uncertainty. Finally, devices installed on the towers have been calibrated under controlled conditions, which quantifies the device uncertainty. These steps are relatively easy to describe but the effort required to quantify and reduce uncertainty to target levels can be considerable. This effort should be expected when installing such a major inflow-monitoring tower. The extensive effort required to quantify the uncertainty is outside the scope of the current paper but will be addressed in future.

II.H. Tower shadowing and flow impact

A tower's own structure will have an unavoidable impact on flow measurements made around the tower. The tower is not completely porous, and so flow is deflected around the tower structure, causing deceleration immediately upstream, and acceleration around the tower. The same effect is seen whenever an object is placed in an otherwise uniform flow.[25] A wake forms downwind of the structure, characterized by reduced wind speeds and high turbulence. These effects can lead to measurable differences between free stream measurements and measurements on the tower. To avoid the wake contaminating data, measurements made when the tower wake region crosses an instrument are usually removed.

To understand the tower's impact on the wind speeds measured with the sonic and cup anemometers, we measured the free stream windspeed approximately 200 m to the west of the M4 tower using a commercial doppler wind LIDAR system. Such LIDAR systems have been shown to give measurements within 2% of sonic anemometer measurements,[26] but in contrast to the tower, LIDAR wind speed measurements are not impacted by any kind of support structure. The LIDAR measured the wind speed in 20-m bins centered at 120 and 140 m above ground. Data from these two bins were then interpolated to 131 m above ground. These interpolated data were then compared to data from a sonic anemometer at that height on the M4 tower (Figure 3(a)). This was carried out during the tower commissioning in May and June of 2011. A comparison was then made between the 131-m sonic anemometer and a cup anemometer at 134 m (Figure 3(b)) using data from the October to November measurement period.

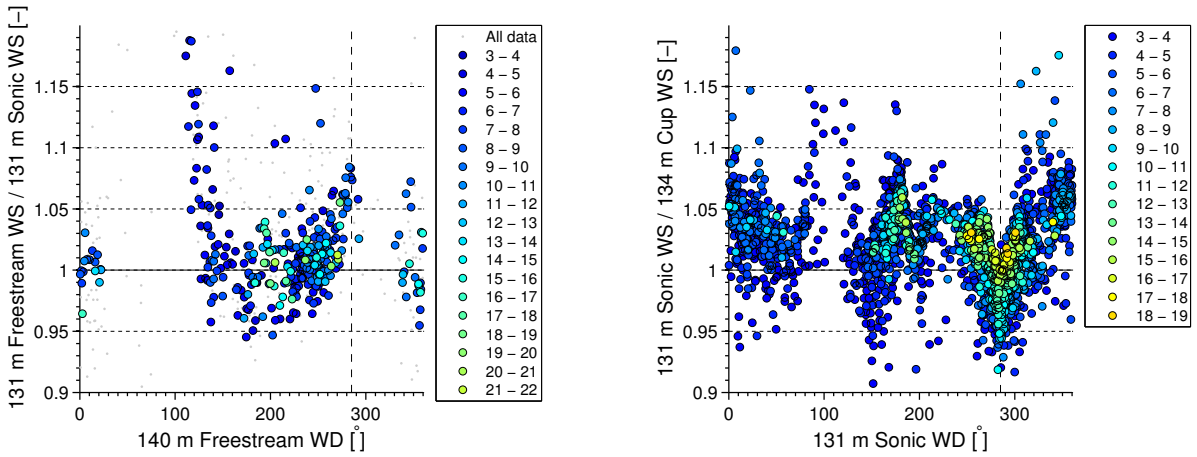

(a) Ratio of freestream LIDAR and sonic anemometer wind speeds at 131 m above ground on the M4 tower. Data are plotted against LIDAR wind direction and grouped by LIDAR wind speed.

(b) Ratio of sonic anemometer wind speeds at 131 m above ground on the M4 tower to cup anemometers at 134 m. Data are plotted against sonic anemometer wind direction and grouped by sonic anemometer wind speed.

Figure 3. Comparison of wind speeds measured by LIDAR, sonic anemometers and cup anemometers on the M4 tower.

Wind speeds measured by the sonic anemometers agree well with the free stream wind speeds measured by the LIDAR (Figure 3(a)). When wind flows through the tower on to the sonics, there is a clear reduction

in wind speed measured by the sonics compared to the free stream. This effect can be seen for winds between approximately 100 and 135°. Assuming that the wake effect is largest when flow approaches the tower from 105° (the opposite direction to the booms) and so the instruments are in the middle of the wake, this implies a 60°-wide wake region. When flows are aligned with the booms (flows from 285°, Figure 3(a)), there may be an increase in the ratio of the wind speed measured in the free-stream to that seen by boom-mounted sonic anemometers, suggesting a slowdown of the flow around the tower at this distance, although the data set does not include many points in this region.

A different trend is seen in Figure 3(b), where measurements from the boom-mounted sonic are compared with cup data. There is a strong decrease in the ratio of the sonic wind speed to the cup wind speed when the flow is aligned with the booms, compared to perpendicular flows. The cup anemometers are mounted on booms with lengths that are 3.5 times the tower face width, while the sonic anemometers are mounted on booms that are 5.8 times as long as the tower face width. Together, this data suggest that the tower modifies the free stream flow, causing flow to slow down some distance from the tower, before accelerating around the tower body. This effect appears to be independent of free stream wind speed. In the one-month data set shown in Figure 3, the effect is well defined using wind speed and flow direction and so could be corrected during post-processing. However the spread in the ratio of winds speeds for a given wind direction would still be approximately 2-3% around a ratio of 1.0. This spread can be considered the noise due to sensor uncertainty and atmospheric effects.

III. Results

On the 11th of October 2011, low surface pressure areas over the Gulf of Alaska, the Canadian Prairies and Newfoundland and high pressure over Colorado led to sustained NW winds across the western United States and the gradual passage of a frontal system from the NW coast into the Midwest. Winds at the NWTC during this period were predominantly from the NW, and wind speeds stayed above 3 m s^{-1} for more than 15 hours (Figure 4). Mean wind directions and Ri_S for each of the 10-minute intervals over which the sonic data were rotated are shown, indicating that the flow was generally from the NW sector during this period, but switched from stable conditions during the night (2:00 UTC to 14:00 UTC, approximately) to convective conditions during the day.

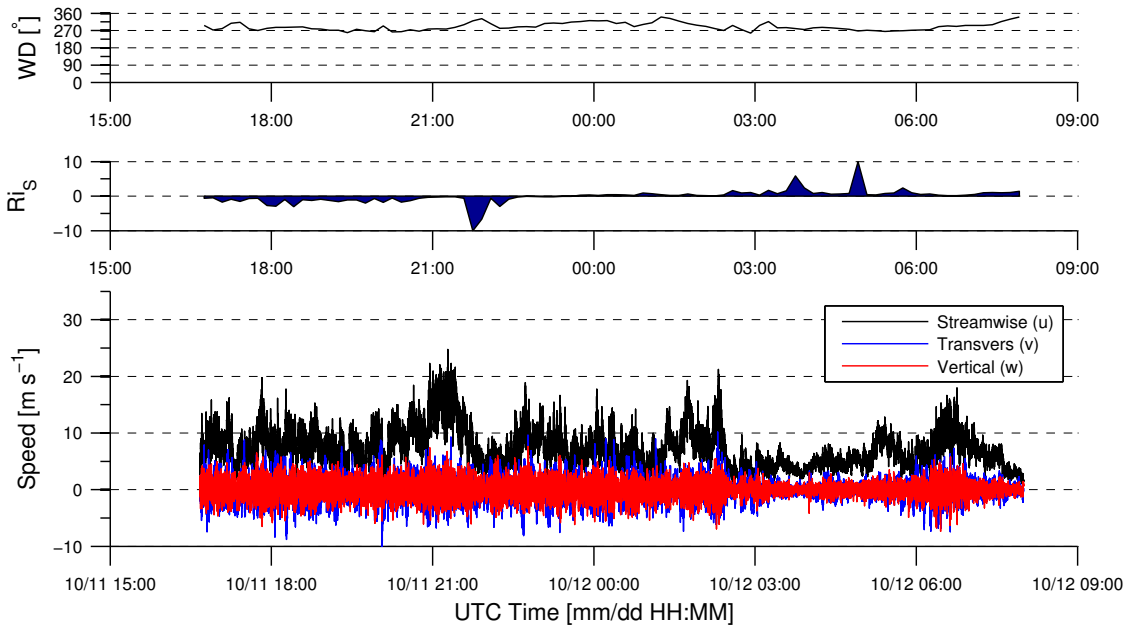

Figure 4. Wind components, Ri_S from 3 to 134 m, and wind direction at 76 m above ground during a 15-hour period starting at 16:40 UTC on October 11, 2011. The velocity component time series is concatenated 10-minute records of 20-Hz data that have been rotated into the mean flow during that interval. WD and Ri_S are the mean values for each 10-minute interval.

A power spectra for the 20-Hz orthogonal velocity components at 76 m above ground during the 15-hour period is shown in Figure 5. A 15-hour time series of orthogonal hub-height wind speeds for this period with 20 Hz resolution was built by concatenating rotated velocity data from the sonic anemometer at 76 m into a single time series (Figure 4). The raw spectra have been smoothed by calculating the log-mean power in each of 5 logarithmically spaced bins per frequency decade, and are plotted on logarithmic scales to show the large variation in both frequency and power. At frequencies below 0.1 Hz, the contribution from the stream-wise component rises more than the transverse, while the power of the vertical component decreases rapidly. The power spectra are identical at frequencies above 0.1 Hz in the inertial subrange, where energy cascades isotropically from larger to smaller scales.

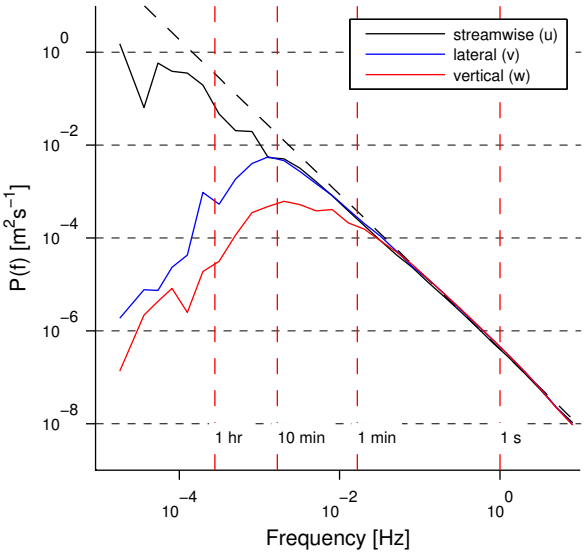

Figure 5. Turbulent velocity component power spectra for the entire period shown in Figure 4.

A spectral gap in the stream-wise flow has been suggested by earlier research.[27,28] The spectral gap would appear as a reduction in power at frequencies below 10 minutes. The presence of the spectral gap in data is sometimes used as justification for the 10-minute averaging period, with the argument being that this averaging period includes the contribution of turbulence only, and not the passage of mesoscale weather systems. The spectral gap is expected to change in size and magnitude depending on terrain (which can contribute to turbulence) and atmospheric forcing.[27,28] However, no spectral gap is seen in these tower measurements even at time periods up to 15 hours. It is likely that the variation in terrain around the tower and strong channeling by the Front Range acts to reduce variation in the stream-wise flow, and thus reduces the effect of synoptic systems that would contribute to the formation of the spectral gap.

The period of strong NW winds shown in Fig. 4 is typical of the wind climate of the NWTC. The strongest winds on site come from the WNW at a direction of approximately 280° to 290°. Winds from the 45° sector from W to NW represent 18% of all winds above 1 m/s at this height. There are secondary peaks in wind frequency to the SSE, and slightly west of north (Figure 6(a)). More detailed analysis using k-means clustering on the 14 years of data available from the M2 tower reveals a strong annual wind cycle, with winds from the NW sector peaking during the winter months and weaker southerly or northerly winds occurring during the summer months.[29]

This paper presents data collected on the 135 m tower during a 4-week period from October 7, 2011 to November 7, 2011. The wind rose of valid data from the M4 tower for this period (Figure 6(b)) is similar to the long-term average, with the most frequent winds from the WNW, which are also the direction of peak wind speeds on site. Data is limited to observations passing the quality control tests described in Section II.F, and so Figure 6(b) is only a representation of valid data, and not a climatology. A secondary peak in wind activity during this time is seen in flows from the SSE, at approximately 175°. Conditions included stable, neutral and unstable stratification, and over the 1-month period show here, less than 3 hours of

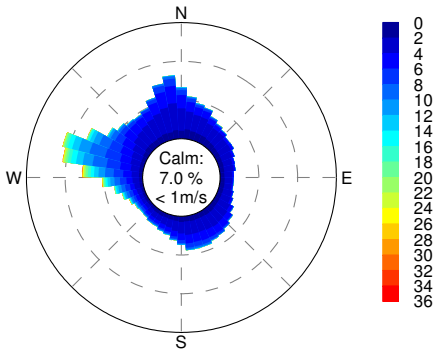

(a) 1996-2011 M2 wind rose (80 m above ground)

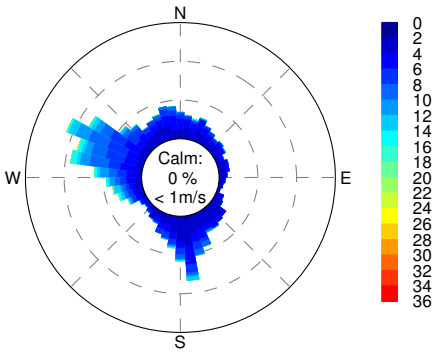

(b) October - November M4 wind rose (76 m above ground)

Figure 6. The frequency and speed of valid measurements of NWTC winds at around 80 m above ground. a) From January 1996 through the end of December 2010 on the M2 tower and b) from 10/7/2011 to 11/7/2011 from the M4 tower. Data are grouped by direction in 7.2° bins and by wind speed in 2 m/s bins. Color bars show wind speeds in 2 m s^{-1} bins.

neutral conditions coincided with wind speeds above 3 ms^{-1}.

III.A. Inflow characteristics

Because of the location of the NWTC at the western edge of the Front Range, winds from different sectors travel across markedly different terrain depending on flow direction. The following sections discuss how the flow structure changes between the WNW and SSE flows at hub height wind speeds between 11 and 13 m s^{-1}, which are typical design wind speeds for large turbines.

III.A.1. Prevailing winds

Flow from the WNW sector (a direction of 285°±15°) at speeds between 11 and 13 m s^{-1} was detected by the sonic anemometer in 71 10-minute intervals during the period from October 7, 2011 to November 7. Using the *Ri* stability classes in Table 2, we found only one 10-minute interval of neutral conditions, or less than 2% of the total. Overall, conditions were unstable in 24% of intervals, slightly stable ('S1') in 4%, stable ('S2') in 46%, and strongly stable ('S3') in the remaining 24%.

A logarithmic increase of mean wind speed with height occurs in all WNW flows at hub-height wind speeds between 11 and 13 m s^{-1} (Figure 7) up to approximately 100 m above ground. This is expected for neutral flows,[18] while stable and unstable flows show a clear departure from the logarithm wind speed profile. Above 100 m, the rate of wind speed increase with height decreases in all stability cases, corresponding to reduced wind shear and a departure from the logarithmic wind profile.[18] Turbulence intensity decreases with height above ground and also in more stable conditions, compared to convective conditions, as has been seen in other studies of the inflow conditions of wind turbines[3] and of the atmospheric boundary layer.[30] Both TKE and peak CTKE are highest in stable conditions (Figure 8) and drop rapidly as stability increases or conditions become unstable.

In the case of flow from the WNW, the integral length scale in the horizontal direction peaks at around 76 m in stable conditions, but continues to increase with height in less stable conditions (Figure 8). This increase in the vertical length scale with height in unstable conditions, compared to stable conditions, reflects the vertical growth of the boundary in unstable (convective) conditions compared to stable conditions. The vertical length scale continues to grow in all conditions, and is of a similar size to the height above ground, which would be expected as the vertical size of eddies is constrained by the ground and the upper edge of the boundary layer. The vertical length scale does increase slightly in convective conditions, compared to stable conditions. Dissipation rate ϵ gradually decreases with height, reaching a minimum at around 100 m in stable conditions, but continues to fall with increasing height in unstable conditions. The minimum level

at about the hub height in stable conditions suggests that wakes will persist longest at the hub, but dissipate more closer to the ground and at the turbine tip. In unstable conditions, wakes will dissipate more rapidly than stable conditions.

III.A.2. Southerly Flows

Southerly flows, from the sector 175°±15°, were less frequent during this period than the WNW flows, with only 17, 10-minute periods where the 76-m wind speed was between 11 and 13 m s^{-1}. Of these flows, 18% were stable ('S2'), while the rest were strongly stable ('S3').

The speed profile of winds from the south shows a similar trend to that from the WNW. During stable conditions, winds have low shear above the 76-m anemometer. Below that height, wind speeds increase relative to winds during slightly stable conditions (Figure 9). The turbulence intensity of the SSE flow is lower than the WNW flows, but shows the same decrease with height as the WNW flows. This reduced turbulence compared to the WNW flow suggests that the increased turbulence seen in the WNW flows is generated by the interaction of the wind and terrain of the Front Range, rather than being generated by buoyancy. The turbulent kinetic energy and coherent TKE are both reduced in comparison to the NW flow, but both TKE and peak CTKE show similar reductions near the ground as stability rises (Figure 10).

The turbulence length scale Λ_u profile of the SSE flow (Figure 10) behaves differently in changing stability conditions than the NNW flows (Figure 8). The length scale of the horizontal flows are markedly increased in strongly stable conditions compared to the slightly stable conditions, which is opposite to the trend seen in the WNW flows, although a maximum is seen in flows from both directions at around 76 m. Vertical length scales appear to peak at around 100 m, in comparison to the WNW flows where vertical length scales continued to increase with increasing height above ground. Dissipation rates for the SSE flows are about half that of the WNW flows, although strongly stable flows are the least dissipative in both cases. Both WNW and SSE flows appear to have a minimum in the dissipation rate profile near 100 m for strongly stable ('S3') conditions.

Observations for this period show that for WNW flows above 3 m s^{-1}, peak CTKE was highest in slightly stable or stable conditions (Fig. 11). The maximum values of TKE and CTKE occurred in the range $0.0 \lesssim Ri_S \lesssim 0.1$. This range is consistent with previous observations at locations in the Great Plains of the United States and in an operating wind farm in California.[31] The large variation in peak CTKE with stability depending on wind direction (compare Figures 8(b) and 10(b)) suggests that at this location during this period, CTKE may be associated with both wind direction and stability, rather than just stability as in simpler sites.

III.B. Choice of stratification measures

As was noted in Section II.E, stratification can be quantified using the normalized Monin-Obukhov Length z/L and the Richardson number, Ri. Both calculations require data from several different instruments.

The Monin-Obukhov length compares the ratio of turbulent kinetic energy produced by shear to that produced by buoyancy. It is calculated from turbulent component and temperature data from sonic anemometers, and from virtual potential temperature from absolute and dew point temperature sensors on the tower (Eq. 18). Over large, flat areas, buoyancy in the boundary layer is driven by the surface heat flux. The surface heat flux $Q_0 = \rho C_p \overline{w'\theta'_v}$ (Figure 12(a)) at the NWTC closely follows the local solar diurnal cycle, peaking during the day and dropping to negative values overnight. The positive heat flux indicates net transfer of heat into the ground. As this diurnal heat flux cycle follows textbook examples[18,32] it also provides a useful check on the data processing routines. The diurnal cycle of z/L follows the heat flux, switching from stable conditions at night to unstable conditions during the day. The number of 10-minute intervals per hour is not constant as data are filtered to remove wind speeds below 3 m s^{-1}.

Although heat fluxes are usually positive during the day and negative at night, this can change depending on surface cover. The daytime stable periods in Figure 12(b) coincided with 24 hours of snowfall followed by snow on the ground for several days, which potentially caused a heat flux into the ground during the day. Similarly, occasional positive heat fluxes during the evening cause infrequent night-time unstable conditions at the hub-height (Figure 12(b)). At the NWTC these night-time unstable conditions could be caused by warm air being convected from upwind of the monitoring towers.

In comparison, layer stability is quantified using the Richardson number. This is based on measurements of wind speed and direction using cups and vanes, and temperature profiles from absolute, differential and

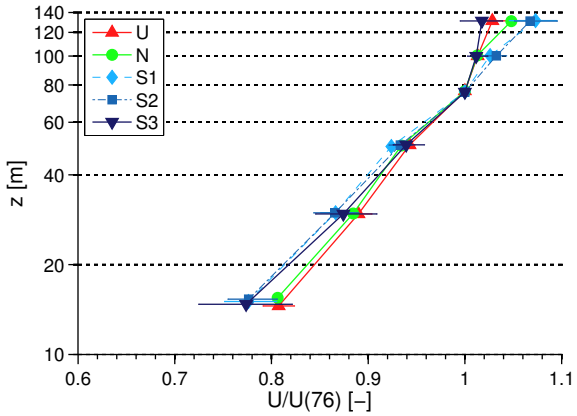

(a) Velocity profile measured by sonic anemometers, normalized by 76-m velocity

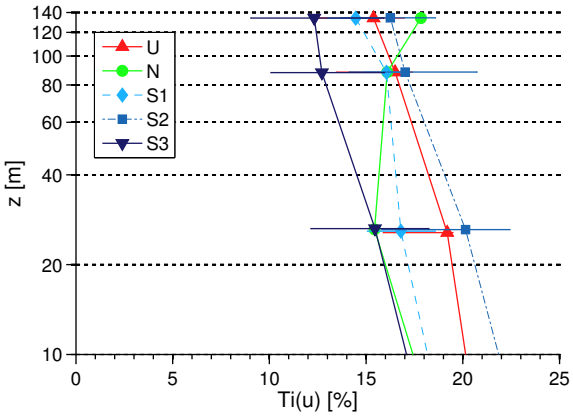

(b) Turbulence intensity measured by cup anemometers

Figure 7. Profiles of velocity and turbulence intensity for WNW flows (285°±15°) at 76-m wind speeds between 11 and 13 m s^{-1} during the period from 10/7/2011 to 11/7/2011. Data are grouped by stability according to the limits in Table 2. Markers are plotted at the mean values at each height. Bars extend from the 25th to 75th percentiles. Markers and bars are displaced by small amounts vertically (less than 1 m) to allow bars to be seen.

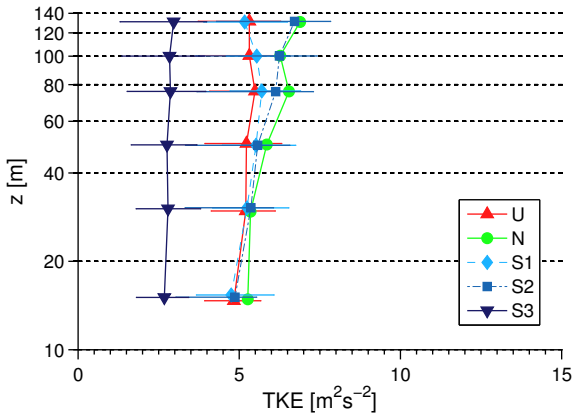

(a) TKE

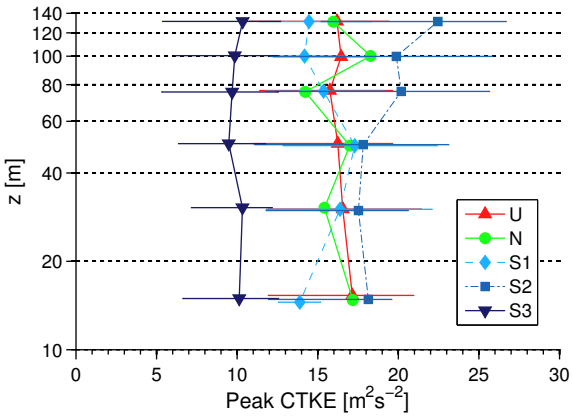

(b) Peak CTKE

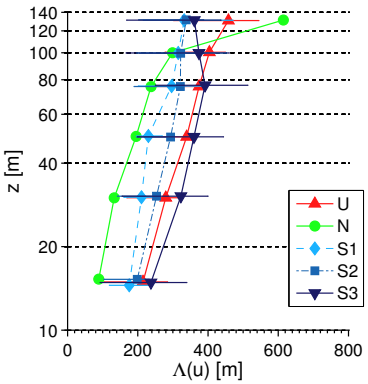

(c) Horizontal turbulence integral length scale

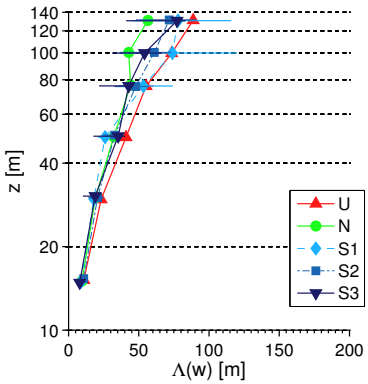

(d) Vertical turbulence integral length scale

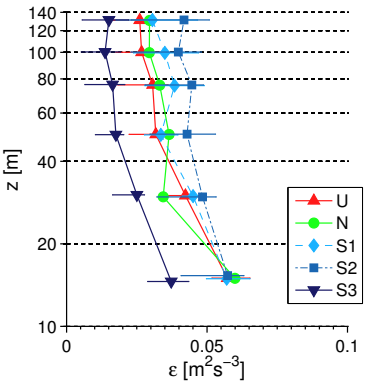

(e) Dissipation rate

Figure 8. Profiles of turbulence and dissipation parameters for WNW flows (285°±15°) at 76-m wind speeds between 11 and 13 m s^{-1}. Plots use the same data and conventions as Figure 7.

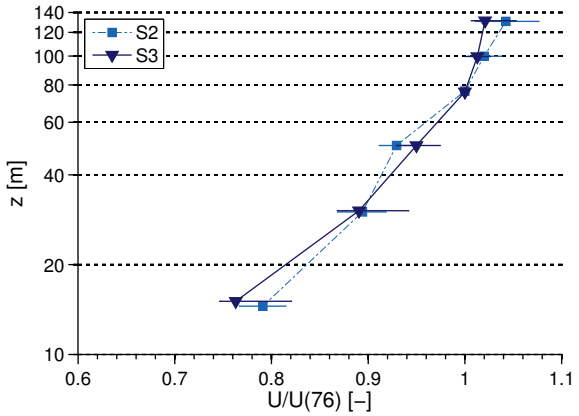

(a) Velocity profile measured by sonic anemometers, normalized by 76-m velocity

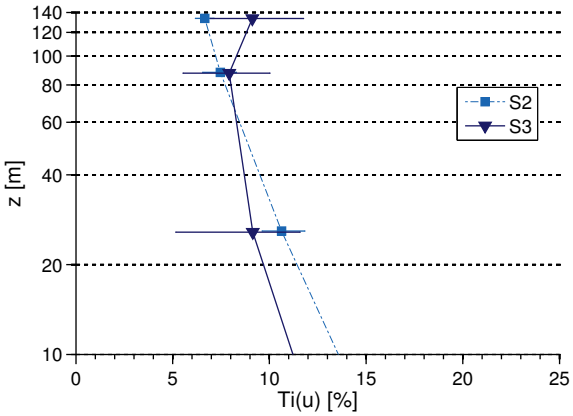

(b) Turbulence intensity measured by cup anemometers

Figure 9. Profiles of velocity and turbulence intensity for SSE flows (175°±15°) at 76-m wind speeds between 11 and 13 m s^{-1} during the period from 10/7/2011 to 11/7/2011. Data are grouped by stability according to the limits in Table 2. Markers are plotted at the mean values at each height. Bars extend from the 25th to 75th percentiles. Markers and bars are displaced by small amounts vertically (less than 1 m) to allow bars to be seen.

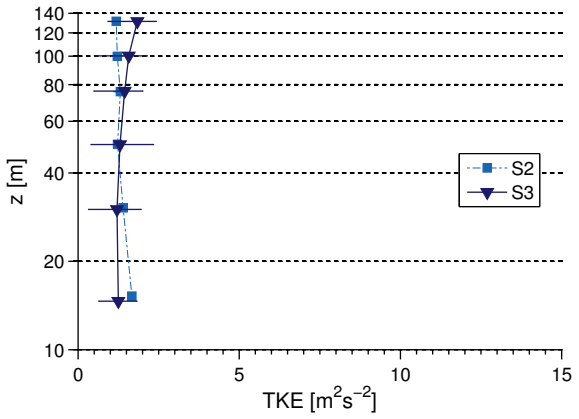

(a) TKE

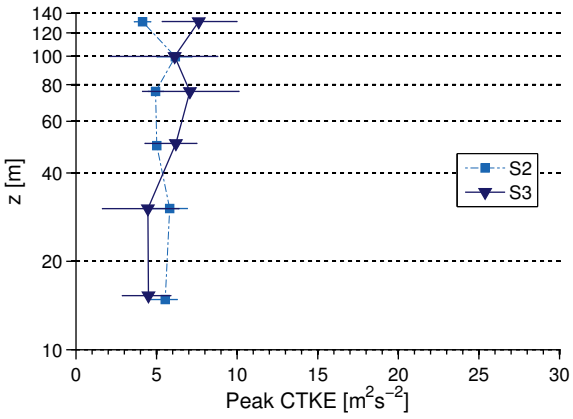

(b) Peak CTKE

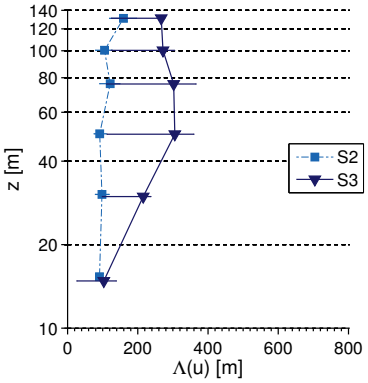

(c) Horizontal turbulence integral length scale

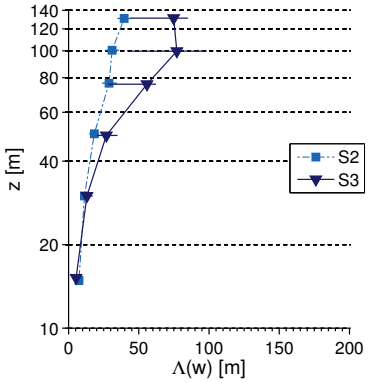

(d) Vertical turbulence integral length scale

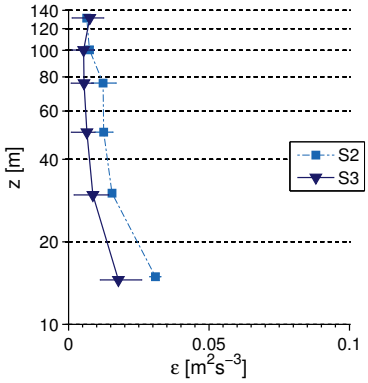

(e) Dissipation rate

Figure 10. Profiles of turbulence and dissipation parameters for SSE flows (175°±15°) at 76-m wind speeds between 11 and 13 m s^{-1}. Plots use the same data and conventions as Figure 9.

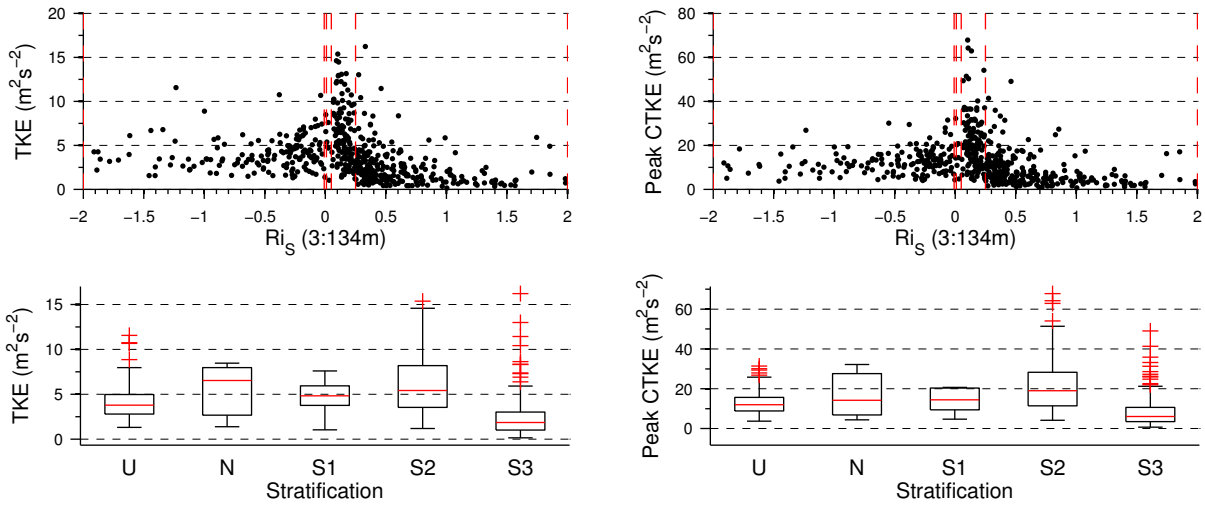

(a) Mean turbulent kinetic energy at 76 m

(b) Peak CTKE at 76 m

Figure 11. Variation of a) mean hub-height turbulent kinetic energy and b) peak hub-height coherent turbulent kinetic energy with $-2 < Ri_S < 2$. Data are limited to 76 m mean wind speeds above 3 m s^{-1} and flows in the WNW sector (285±15°). Data are 10-minute average values obtained during the period from 10/7/2011 to 11/7/2011.

dew point temperature sensors (Eq. 19 and 20), and has been used in previous investigations of wind turbine performance.[3,4] At the NWTC from early October 2011 to early November 2011 the Richardson number indicated stable conditions overnight, switching to unstable conditions during the day (Fig. 12(b)). The pattern of stable nights and unstable days agrees with the cycle from the Monin-Obukhov length.

The occasional difference between layer stability quantified using Ri_S and local stability quantified using z/L reflects the complex stratification that may exist at this site. It is possible that a stable layer might overlay an unstable layer (or vice versa) for a short period of time, which can cause apparent differences in layer versus local stratification.

The two Richardson numbers that were defined in Section II.E always agree in sign (Figure 13(a)), but not in magnitude. This difference in magnitude but not sign is explained by a comparison of Eq. (19) and (20), as $(du_m/dz)^2 + (dv_m/dz)^2$ is always greater than $(dU/dz)^2$, and it is likely that there will be a small amount of directional veer between the ground and 134 m. Comparing Ri with z/L (Figure 13(b)) shows that the two measures do not always give the same stability, which is also seen in Figure 12(b). There is also wide scatter around the Businger-Dyer relationships (Eq. 21), which were generated from analysis of measurements over flat and uniform surfaces[33] and have been confirmed by other measurements.[20] Because the terrain upwind of the NWTC is not flat or uniform, more turbulence is generated mechanically than over flat, uniform terrain, particularly in the vertical and transverse directions. This modification of the turbulence leads to large scatter compared to flat-field reference cases. This difference may not be as large on sites with longer upwind fetch or more uniform terrain.

III.C. Implications for other sites

Modern utility-scale turbines frequently have hubs at 80 m above ground or higher, and rotor disks of 80-m diameter or larger. Figures 7, 8, 9, and 10 suggest that in this particular location, for flows from the WNW and SSE and at this speed, turbines extend out of the surface layer where flows are strongly influenced by the surface and into a different region of the atmosphere. Because of the change in gradients at around 80 m, extrapolation from measurements at lower elevations to the turbine hub height will be prone to error, particularly velocity profiles in stable conditions. Although the change in velocity profile and turbulence that we see at the NWTC might not occur at all sites at this height, this behavior cannot be known *a priori*. This uncertainty is a strong argument for a careful survey of the atmosphere using direct measurement rather than extrapolation as part of the wind resource assessment process.

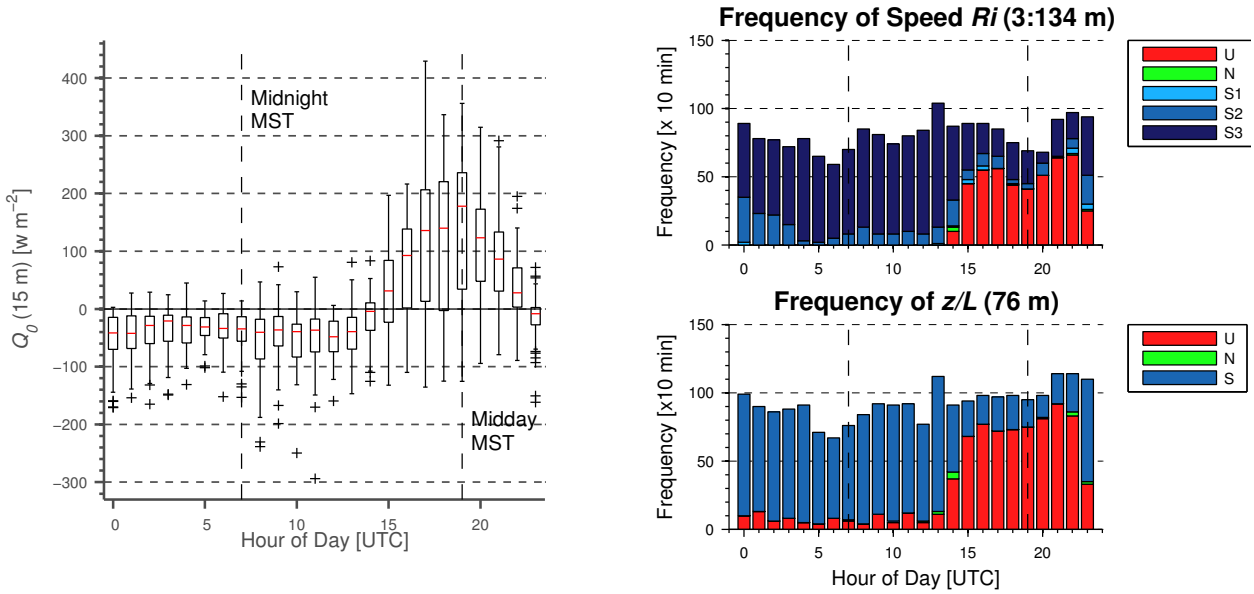

(a) Diurnal heat flux cycle

(b) Diurnal stability cycle

Figure 12. Diurnal cycles of a) Heat flux Q_0 at 15 m and b) Ri_S from 3 to 134 m and z/L at 76 m. Stability classes shown in (b) are listed in Table 2. Data are 10-minute average values from 10/7/2011 to 11/7/2011 for 76 m wind speeds above 3 m s^{-1}. Data include all wind directions except the tower wake (105° ± 30°).

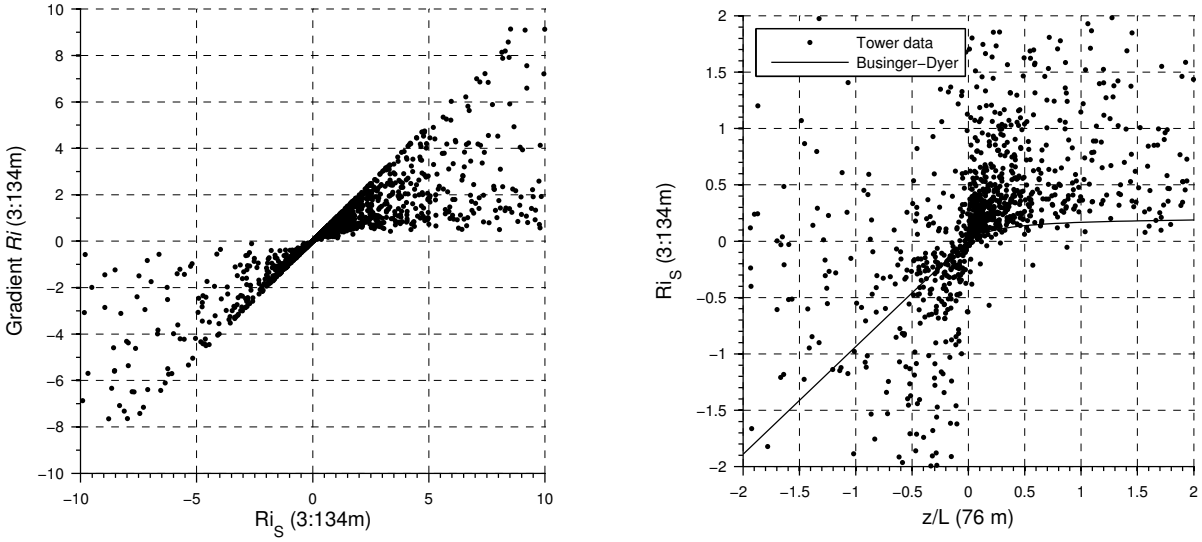

(a) Comparison of Richardson numbers calculated with (Gradient Ri) and without directional shear (Ri_S, also Speed Ri).

(b) Comparison of Speed Richardson number Ri_S and normalized hub-height Monin-Obukhov Length z/L.

Figure 13. Comparison of the layer stability measures (a) Ri and Ri_S and (b) layer stability measure Ri_S with the local stability measure z/L on the tower. The Businger-Dyer relationship between Ri_S and z/L (Eq. 21) is shown for reference. Data are limited to 76 m mean wind speeds over 3 m s^{-1}. Data include all wind directions except the tower wake (105° ± 30°).

Vertical profiles of the wind speed, turbulence and dissipation rate also show that there are significant differences between conditions that a turbine experiences, as stability changes but wind speed and direction stay constant. Figures 7, 8, 9 and 10 show that TKE can vary by a factor two between strongly stable and unstable conditions, while TKE and peak CTKE are both highest in low Ri_S conditions that are also linked to high turbine loads. Stability, TKE, peak CTKE, and dissipation all influence wake propagation and so including their real values or probability distributions in a site optimization process may lead to improved turbine siting.

The relative insensitivity of the Richardson number to local effects, compared to Monin-Obukhov length (Figures 12(b) and 13(b)), is a good argument for the use of the Richardson number to quantify flows when considering the interaction of a turbine with the wind. Another reason to use the Richardson number is that the Richardson number integrates conditions over the entire height of the turbine, and the turbine uses all of the flow through the turbine rotor to produce power. In comparison, the Monin-Obukhov length L uses data measured at a few discrete heights. The Richardson number can be calculated from data taken at 1 Hz by cup anemometers, wind vanes, differential temperature sensors, and humidity sensors, and so meaningful stability data can be obtained as part of a typical wind resource assessment campaign.

IV. Conclusion

Designing and instrumenting a measurement mast for inflow characterization requires careful consideration of the measurement goals and flow characteristics. At the National Wind Technology Center, two new 135-m meteorological towers have been instrumented with sonic anemometers, temperature sensors, cup anemometers, and wind vanes. Importantly, data from the inflow towers and turbines at the NWTC are all timestamped with time signals from GPS satellites, allowing measurements to be synchronized.

The NWTC measurement suite allows inflow mean conditions and turbulence to be quantified as well as local and layer stability. This high-resolution data set will be used to investigate atmospheric conditions when high turbine loads occur; to investigate links between turbulence and stability; to further validate the stochastic flow model TurbSim;[11] for comparison with remote sensing instrumentation,[16] and as test data for nacelle-mounted LIDAR turbine control techniques.[34]

First data from the new 135-m tower in October and November 2011 show that wind conditions vary considerably depending on wind direction and atmospheric stability. For the same wind speeds, as conditions become strongly stable, wind shear increases but turbulence intensity and dissipation rate decreases compared to unstable conditions. The change in dissipation rate will be important for the duration of wakes downstream of operational turbines, resulting in more persistent wakes in stable, nighttime conditions. Wind speed, turbulence, dissipation and length scales all show different vertical profiles depending on wind direction. TKE, peak CTKE and the dissipation rate ϵ in flows from the same direction all peak under slightly stable conditions, supporting previous studies. Results also show changes in wind speed gradients at or near turbine hub heights (80 to 100 m above ground). Therefore, incorrect estimates of turbine hub or rotor disk conditions would be made if data are extrapolated from lower-level data, such as 60- or 80-m-tall towers.

The data resulting from the long-term operation of these towers and turbines will be crucial for validating existing aerostructural design models for multi-megawatt turbines, and for developing improved models for designing larger, more efficient next-generation turbines.

Acknowledgments

This work was carried out with the support of the DOE/EERE Wind and Water Program.

References

[1]Bolinger, M. and Wiser, R., "Understanding Trends in Wind Turbine Prices Over the Past Decade," Tech. Rep. LBNL-5119E, Lawrence Berkeley National Laboratory, 2011.

[2]Hansen, K. S. and Larsen, G. C., "Characterising Turbulence Intensity for Fatigue Load Analysis of Wind Turbines," *Wind Engineering*, Vol. 29, No. 4, June 2005, pp. 219–329.

[3]Wharton, S. and Lundquist, J., "Assessing atmospheric stability and its impacts on rotor-disk wind characteristics at an onshore windfarm," *Wind Energy*, 2011.

[4]Hand, M., Kelley, N. D., and Balas, M., "Identification of Wind Turbine Response to Turbulent Inflow Structures," Tech. rep., NRELCP-500-33465, 2003.

[5]Kaimal, J. and Wyngaard, J., "The Kansas and Minnesota Experiments," *Boundary-Layer Meteorology*, Vol. 50, March 1990, pp. 31–47.

[6]Mücke, T., Kleinhans, D., and Peinke, J., "atmospheric turbulence and its influence on the alternating loads on wind turbines," *Wind Energy*, Vol. 14, 2011, pp. 301–316.

[7]Kelley, N. D., "The Identification of Inflow Fluid Dynamics Parameters That Can Be Used to Scale Fatigue Loading Spectra of Wind Turbine Structural Components," Tech. Rep. TP-442-6008, NREL, 1993.

[8]Hand, M. M., Robinson, M. C., and Balas, M. J., "Wind turbine response to Analytic Inflow Vortex Parameters Variation," Tech. Rep. CP-500-34297, NREL, 2003.

[9]Kelley, N. D., Jonkman, B. J., and Scott, G. N., "Great Plains Turbulence Environment: Its Origins, Impact, and Simulation." Tech. Rep. CP-500-40176, NREL, 2006.

[10]Kelley, N. D., Shirazi, M., Jager, D., Wilde, S., Adams, J., Buhl, M., Sullivan, P., and Patton, E., "Lamar Low-Level Jet Program Interim Report," Tech. Rep. TP-500-34593, NREL, 2004.

[11]Kelley, N. D. and Jonkman, B. J., "Overview of the TurbSim Stochastic Inflow Turbulence Simulator: Version 1.21 (Revised February 1, 2001)." Tech. Rep. TP-500-41137, NREL, 2007.

[12]Kelley, N. D., "Turbulence-Turbine Interaction: The Basis for the Development of the TurbSim Stochastic Simulator." Tech. Rep. TP-5000-52353, National Renewable Energy Laboratory, 2011.

[13]Banta, R., Olivier, L., and Gudiksen, P., "Sampling requirements for drainage flows that transport atmospheric contaminants in complex terrain," *Radiation Protection Dosimetry*, Vol. 50, No. 2-4, 1993, pp. 243–248.

[14]Kelley, N. D., "Optimization of Sodar Wind Profile Measurements in Low-Humidity Climates at High Altitudes: Cooperative Research and Development Final Report, CRADA number CRD-07-00246." Tech. Rep. TP-7A1-48410, NREL, 2010.

[15]Frehlich, R. and Kelley, N., "Measurements of Wind and Turbulence Profiles With Scanning Doppler Lidar for Wind Energy Applications," *Selected Topics in Applied Earth Observations and Remote Sensing, IEEE Journal of*, Vol. 1, No. 1, march 2008, pp. 42 –47.

[16]Friedrich, K., Lundquist, J. K., Aitken, M., Kalina, E. A., and Marshall, R. F., "Stability and Turbulence in the Atmospheric Boundary Layer: An Intercomparison of Remote Sensing and Tower Observations," *Geophysical Research Letters*, Submitted, 2011, pp. 17.

[17]Wilczak, J., Oncley, S., and Stage, S., "Sonic Anemometer Tilt Correction Algorithms," *Boundary-Layer Meteorology*, Vol. 99, 2001, pp. 127–150, 10.1023/A:1018966204465.

[18]Stull, R., *An Introduction to Boundary Layer Meteorology*, Kluwer Academic Publishers, 2nd ed., 1988.

[19]Garratt, J., *The Atmospheric Boundary Layer*, Cambridge Atmospheric and Space Science Series, Cambridge University Press, 1st ed., 1994.

[20]Oncley, S. P., a. Friehe, C., Larue, J. C., Businger, J. A., Itsweire, E. C., and Chang, S. S., "Surface-layer Fluxes, Profiles and Turbulence Measurements over Uniform Terrain under Near-Neutral Conditions," *Journal of the atmospheric Sciences*, Vol. 53, No. 7, 1996, pp. 1029–1044.

[21]Businger, J. A., Wyngaard, J. C., Izumi, Y., and Bradley, E. F., "Flux-Profile Relationships in the Atmospheric Surface Layer," *Journal of the Atmospheric Sciences*, Vol. 28, No. 2, 2011/10/27 1971, pp. 181–189.

[22]Grachev, A. A. and Fairall, C. W., "Dependence of the Monin–Obukhov Stability Parameter on the Bulk Richardson Number over the Ocean," *Journal of Applied Meteorology*, Vol. 36, No. 4, 2011/10/01 1997, pp. 406–414.

[23]Vickers, D. and Mahrt, L., "Evaluating Formulations of Stable Boundary Layer Height," *Journal of Applied Meteorology*, Vol. 43, No. 11, 2011/10/01 2004, pp. 1736–1749.

[24]Barthelmie, R. J. and Jensen, L. E., "Evaluation of wind farm efficiency and wind turbine wakes at the Nysted offshore wind farm," *Wind Energy*, Vol. 13, No. 6, 2010, pp. 573–586.

[25]Kundu, P. and Cohen, I., *Fluid Mechanics*, Elsevier, 3rd ed., 2004.

[26]Sathe, A., Mann, J., Gottschall, J., and Courtney, M. S., "Can Wind Lidars Measure Turbulence?" *Journal of Atmospheric and Oceanic Technology*, Vol. 28, July 2011, pp. 853 – 868.

[27]Van der Hoven, I., "Power Spectrum Of Horizontal Wind Speed In The Frequency Range From 0.0007 To 900 Cycles Per Hour," *Journal of Meteorology*, Vol. 14, No. 2, 2011/11/01 1957, pp. 160–164.

[28]Smedman-Högström, A.-S. and Högström, U., "Spectral Gap in Surface-Layer Measurements," *Journal of the Atmospheric Sciences*, Vol. 32, No. 2, 2011/11/01 1975, pp. 340–350.

[29]Clifton, A. and Lundquist, J., "Data clustering reveals climate impacts on local wind phenomena," *Journal of Applied Meteorology and Climatology*, Submitted 2011.

[30]Kaimal, J. and Finnigan, J., *Atmospheric Boundary Layer Flows their Structure and Measurement*, Oxford University Press Inc. New York, 1994.

[31]Kelley, N. D., Jonkman, B. J., Scott, G. N., Bialasiewicz, J., and Redmond, L., "The impact of coherent turbulence on wind turbine aeroelastic response and its simulation," Tech. Rep. NREL/CP-500-38074, NREL, 2005.

[32]Oke, T. R., *Boundary Layer climates*, Methuen, London, 1988.

[33]Businger, J. A., "Turbulent transfer in the atmospheric surface layer," *Workshop on Micrometeorology*, edited by N. E. Busch and D. A. Haugen, American Meteorological Society, 1973, pp. 67–100.

[34]Pao, L. Y. and Johnson, K., "Control of Wind Turbines," *Control Systems, IEEE*, Vol. 31, No. 2, April 2011, pp. 44–62.